

Powering Lithium–Sulfur Battery Performance by Propelling Polysulfide Redox at Sulfophilic Hosts

Zhe Yuan,[†] Hong-Jie Peng,[†] Ting-Zheng Hou,[†] Jia-Qi Huang,[†] Cheng-Meng Chen,[‡] Dai-Wei Wang,[†] Xin-Bing Cheng,[†] Fei Wei,[†] and Qiang Zhang^{*,†}

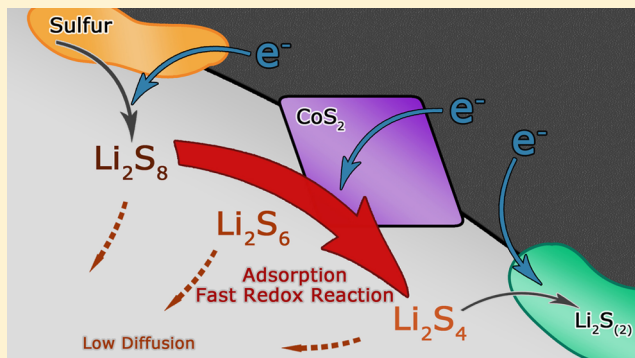
[†] Beijing Key Laboratory of Green Chemical Reaction Engineering and Technology, Department of Chemical Engineering, Tsinghua University, Beijing 100084, China

[‡] Key Laboratory of Carbon Materials, Institute of Coal Chemistry, Chinese Academy of Sciences, 27 Taoyuan South Road, Taiyuan 030001, China

Supporting Information

ABSTRACT: Lithium–sulfur (Li–S) battery system is endowed with tremendous energy density, resulting from the complex sulfur electrochemistry involving multielectron redox reactions and phase transformations. Originated from the slow redox kinetics of polysulfide intermediates, the flood of polysulfides in the batteries during cycling induced low sulfur utilization, severe polarization, low energy efficiency, deteriorated polysulfide shuttle, and short cycling life. Herein, sulfophilic cobalt disulfide (CoS_2) was incorporated into carbon/sulfur cathodes, introducing strong interaction between lithium polysulfides and CoS_2 under working conditions. The interfaces between CoS_2 and electrolyte served as strong adsorption and activation sites for polar polysulfides and therefore accelerated redox reactions of polysulfides. The high polysulfide reactivity not only guaranteed effective polarization mitigation and promoted energy efficiency by 10% but also promised high discharge capacity and stable cycling performance during 2000 cycles. A slow capacity decay rate of 0.034%/cycle at 2.0 C and a high initial capacity of 1368 mAh g^{-1} at 0.5 C were achieved. Since the propelling redox reaction is not limited to Li–S system, we foresee the reported strategy herein can be applied in other high-power devices through the systems with controllable redox reactions.

KEYWORDS: Lithium–sulfur batteries, polysulfide, redox reaction, cathode, carbon



High-energy-density rechargeable batteries are of paramount interest and under vigorous investigation because of the ubiquitous demand of energy storage devices in flourishing sustainable fields of electric vehicles, portable electronic devices, and renewable energy harvesting at a large scale. The lithium–sulfur (Li–S) battery is recognized as a promising alternative for conventional Li-ion batteries due to the high theoretical energy density of $\sim 2600 \text{ Wh kg}^{-1}$ (based on overall reaction, $\text{S}_8 + 16\text{Li} \leftrightarrow 8\text{Li}_2\text{S}$).^{1,2} Elemental sulfur provides a theoretical capacity of 1672 mAh g^{-1} through the multielectron redox conversion involving multiphase transformation, far exceeding that of intercalation-type cathode materials.^{3–6} Meanwhile, sulfur has the advantages of low cost, natural abundance, and environmental friendliness.

Direct lithiation of sulfur into insoluble reduction products (Li_2S_2 and Li_2S) via a solid–solid route is kinetically sluggish due to the insulating nature of these solid compounds. Aprotic electrolytes are thereby adopted to dissolve soluble intermediates and facilitate the solid–liquid conversion. Hence, the redox of polysulfides in liquid phase, namely, $\text{Li}_2\text{S}_8 \leftrightarrow \text{Li}_2\text{S}_6 \leftrightarrow \text{Li}_2\text{S}_4$, which connects the two solid phases of sulfur and $\text{Li}_2\text{S}_2/\text{Li}_2\text{S}$, is virtually the kernel of sulfur redox chemistry in aprotic

electrolyte (Figure 1a). The corresponding transport of electrons demands the participation of conductive substrates. Therefore, many conductive hosts,^{7,8} e.g., porous carbon,^{9–12} graphene and its derivatives,^{13–16} carbon nanotubes,^{17–19} conductive polymers,^{20–22} and their hybrids^{23,24} have been employed to load sulfur and to improve the electrochemical performance of Li–S batteries, due to their appreciable conductivity, surface area, and void space to accommodate the volume fluctuation. However, the appearance of soluble and mobile redox species gives rise to other problems. Once oxidized or reduced to soluble and high-polar polysulfides, sulfur species lose intimate electrical contact with conductive matrix due to their poor affinity, resulting in high charge transfer resistance and slow redox kinetics for polysulfide redox reactions.²⁵ The dissolution of polysulfide intermediates (Li_2S_x , $4 \leq x \leq 8$) leads to severe shuttle effect,²⁶ causing anode corrosion, a low Coulombic efficiency, and diminished capacity.

Received: October 13, 2015

Revised: December 24, 2015

Published: December 29, 2015



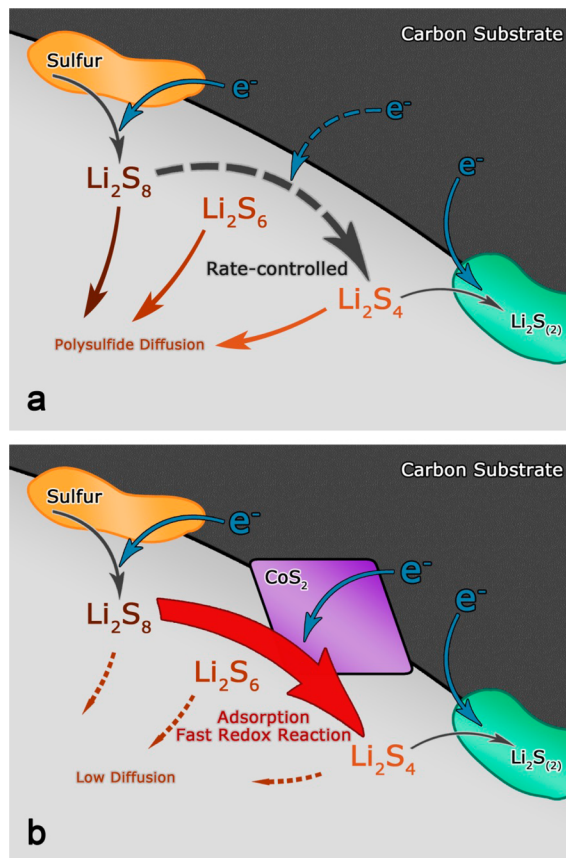


Figure 1. Schematic illustration of the discharge process in sulfur cathodes. (a) Pure carbon/sulfur cathode where polysulfide reduction is rate-controlled and polysulfide diffusion is dominated and (b) CoS_2 -incorporated carbon/sulfur cathode where polysulfide reduction is accelerated and polysulfide diffusion is weakened.

Driven by the concentration difference, dissolved lithium polysulfides are transported to the anode, membrane, and dead zone in the cell, and consequently react with the lithium anode or disproportionate in the electrolyte, therefore irreversibly being deposited or consumed. The use of functional interlayers,^{17,27–30} anode-protective additives,^{31,32} and novel electrolyte configurations^{33,34} are proposed to mitigate polysulfide diffusion or to prevent parasitic reactions between polysulfides and lithium metal anode.

The aforementioned strategies, namely, preventing the diffusion and nonelectrochemical reactions of polysulfides, are the mainstream for tackling the “shuttle” issue. However, the flooding of polysulfides in a cell should not only be owing to their arbitrary while thermodynamically inevitable diffusion, but also to the slow redox of polysulfides as well as their accumulation in the electrolyte. Only if a polysulfide molecule was adsorbed on conductive substrate, the liquid-involving polysulfide redox would be electrochemically available. However, the high polarity of polysulfides reduces their affinity with typically nonpolar hosts such as carbon. The flooding of polysulfides is similar to an actual flood. It is common sense that digging canals and widening/deepening existing channels are more effective approaches to alleviating the deluge, compared to blocking the deluge with dams, dikes, and embankments. Similarly, rather than blocking the dissolution and diffusion of polysulfides, accelerating polysulfide conversion through enhanced polysulfide redox is another

promising strategy to suppress the notorious flooding of polysulfides and to enhance the energy output and efficiency, as well as the cycle life of sulfur cathodes.

A few pioneer researches have been carried out to enhance the polysulfide redox. Very recently, Nazar and co-workers proposed strong polysulfide/ Li_2S binding with Magnéti-phase Ti_4O_7 host and surface-mediated redox chemistry to enhancing Li-S reaction.³⁵ The use of entrapped polysulfides in the cathode that relies on MnO_2 nanosheets reacting with initially formed lithium polysulfides to catenate and bind them and converting them to insoluble Li_2S via disproportionation were also explored.³⁶ Similarly, Cui et al. demonstrated that a hybrid electrode surface of carbon/tin-doped indium oxide (ITO) could enhance the redox kinetics of polysulfides and mediate their deposition.³⁷ Two-dimensional (2D) metal disulfide nanomaterials were also applied for encapsulating Li_2S cathodes or facilitating the performance of a polysulfide catholyte in the same principle.^{38,39} Chiang and co-workers first reported the precipitation of Li_2S proceeds through nucleation followed by 2D growth.⁴⁰ Very recently, high-surface-area Co_9S_8 with hierarchical porosity was proposed by Pang et al. to afford superior LiPS adsorptivity for long-life and high-loading Li-S batteries.⁴¹ Although it is noted that the heteropolar feature of conductive surface favors the charge transfer from host material to polysulfides, the mechanism in which the polar surface accelerates polysulfide redox has not been clearly revealed yet.

In this contribution, cobalt disulfide (CoS_2 , cattierite), an earth-abundant mineral sharing pyrite-type crystal form, served as conductive sulfophilic host to propel polysulfide redox in aprotic electrolyte. Half-metallic CoS_2 possesses an appreciable conductivity of $6.7 \times 10^3 \text{ S cm}^{-1}$ at 300 K,⁴² which far exceeds those of other semiconducting first-row transition metal disulfides such as FeS_2 and NiS_2 , allowing CoS_2 to afford efficient electron pathways and high electrocatalytic activity for polysulfide redox reactions in aqueous solutions.^{43,44} The incorporation of CoS_2 can significantly enhance the redox reactivity of lithium polysulfides due to their strong chemical affinity (Figure 1b). The accelerated polysulfide redox kinetics, confirmed by electrochemical evidence, promised low polarization and high energy efficiency under high current densities, as well as excellent cyclic performance. A ~60% promotion in discharge capacity and a ~10% raise in energy efficiency were achieved under the participation of CoS_2 for composites containing 75 wt % sulfur, and a slow capacity decay rate of 0.034%/cycle was realized at 2.0 C within 2000 cycles.

The CoS_2 sample was synthesized via a simple and facile hydrothermal method. The as-synthesized CoS_2 exhibits micron-sized cluster-like morphology that is composed of bipyramid primary particles with sizes ranging from 20 to 200 nm (Figure S1a). Since the pyrite-type CoS_2 possesses a face-centered cubic crystal structure, the exposed surface of a primary particle should be dominantly (111) plane, which is further verified by a lattice spacing of 0.32 nm and corresponding fast Fourier transform (FFT) pattern (Figure S2a). As the X-ray diffraction (XRD) pattern indicated (Figure S2b), the hydrothermally synthesized CoS_2 displays a typical pyrite-type structure, where CoS_6 octahedrons interconnect by sharing the corner sulfur atoms. The CoS_2 was mechanically milled with graphene prepared by thermal reduction to form CoS_2 /graphene composite (denoted as $\text{CoS}_2 + G$). In the composite, the CoS_2 clusters of $\sim 1 \mu\text{m}$ in size are attached to highly crumpled graphene substrate, forming electron pathways from conductive framework to heteropolar CoS_2 surface

(Figure S1b). Note that the microsized feature of CoS_2 primary particles limits their uniformity within graphene framework, which ought to be a future direction for further improvements (Figure S1c). However, the scope of this paper is to illustrate the intrinsic enhancement for Li–S batteries through a bulk and raw material of CoS_2 rather than the nanostructuring effect. The specific surface area of CoS_2 was as low as $1.38 \text{ m}^2 \text{ g}^{-1}$ (Figure S3), which was almost negligible compared to graphene ($>700 \text{ m}^2 \text{ g}^{-1}$). Therefore, major conducting substrate in the composite for Li–S batteries is still graphene nanosheets.

To confirm the strong CoS_2 –polysulfide interaction, Li_2S_4 (in nominal formulation) of 10.0 mmol L^{-1} dissolved in 1,2-dimethoxyethane (DME) was chosen to model high-polar lithium polysulfides as the adsorbate for static adsorption. Graphene and CoS_2 of equal surface area (0.30 m^2) were added into Li_2S_4 /DME solutions as adsorbents, followed by vigorous stirring and centrifugation. As shown in Figure 2a, CoS_2

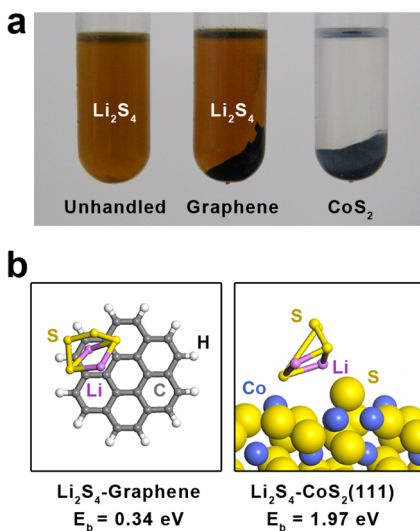


Figure 2. Strong static interaction between CoS_2 and lithium polysulfide. (a) Visualized adsorption of Li_2S_4 on graphene and pristine CoS_2 with the same surface area. (b) Binding geometries and energies of a Li_2S_4 molecule on graphene (left, modeled as coronene) and (111) plane of CoS_2 with cobalt-terminated surface (right), which is derived from theoretical calculation based on DFT.

thoroughly decolored dissolved polysulfides, while graphene had no observable effect on the Li_2S_4 /DME solution since the tawny color remained the same. The sharp contrast suggests significantly promoted affinity of Li_2S_4 molecules to heteropolar CoS_2 with ionic bonding of Co–S than nonpolar graphene. But note that the surface area of CoS_2 is formidably lower than graphene. The overall adsorption of dissolved polysulfides from bulk electrolytes was not enhanced by adding 30 wt % of CoS_2 into the composites, which varies significantly from porous and polar adsorptive materials reported previously (Figure S4).^{45,46} Therefore, the affinity of CoS_2 to polar polysulfides affords strong adsorbate–adsorbent interaction at an interfacial scale rather than preventing the leakage of polysulfides into the electrolyte by chemical adsorption in the view of the whole cell. Compared to nonpolar graphene, CoS_2 with heteropolar surface favors the adsorption of polysulfides onto conductive matrix and subsequent electrochemically driven charge transfer at a nanoscale interface.

The nanoscale interfacial interactions between CoS_2 and lithium polysulfides were further validated from a computa-

tional perspective. First-principle calculations based on density functional theory (DFT) were conducted to obtain the binding geometries and energies of a Li_2S_4 molecule on different substrates, where graphene was modeled as coronene, while an infinite (111) stripes of CoS_2 with terminated cobalt atoms mimicked the exposed surface of as-synthesized octahedral CoS_2 particles. The binding energies of Li_2S_4 to graphene basal plane or (111) plane of CoS_2 are dramatically different (Figure 2b). Graphene, formed mainly by nonpolar C–C bond, only provides a limited binding energy of 0.34 eV . Impressively, an elevated binding energy of 1.97 eV is generated between CoS_2 and Li_2S_4 . The cyclic Li_2S_4 molecule follows certain orientation in order to achieve lowest overall energy under optimized configuration. Driven by the electrostatic affinities of donor–acceptor pairs, lithium atoms and terminal sulfur atoms of Li_2S_4 come adjacent to sulfur dimers and cobalt atoms of CoS_2 , respectively (Figure 2b and S5). In the meantime, the S–S bridge of Li_2S_4 turns over to the far end from CoS_2 surface plane, allowing atoms with large charge density to reach the near vicinity of “sulfophilic” CoS_2 surface and thereby, producing sufficient charge transfer and large binding energy at a molecular level. On the contrary, graphene surface does not possess a polarized charge distribution, which results in low atomic interaction and inferior binding energy.

The strong interfacial interaction between CoS_2 and polysulfides may impose two major impacts on sulfur chemistry in aprotic electrolyte: (1) enhancing the retention of polysulfides in the cathode by chemical adsorption and (2) favoring the charge transfer from conductive matrix to adsorb polysulfides and corresponding polysulfide redox. However, the former one would be neglected due to the extremely limited surface area of heteropolar CoS_2 in the whole composite. Therefore, symmetrical cells were designed by sandwiching Li_2S_6 -containing electrolytes between two identical electrodes to investigate the redox kinetics of polysulfides (see Methods). Graphene and two $\text{CoS}_2 + \text{G}$ composites with different weight ratios (denoted as CoS_2 (15%) + G, and CoS_2 (30%) + G, respectively) served as host materials in the electrodes. The open circuit voltages of such symmetrical cells were 0 V.

Cyclic voltammetric (CV) tests were performed within a voltage window of -0.7 to 0.7 V for symmetrical Li_2S_6 – Li_2S_6 cells. The polarization profiles present major fraction of redox current of Li_2S_6 , and minor contribution of capacitive current as indicated by the Li_2S_6 -free symmetrical cells (Figure 3a). It can be clearly observed that the current density significantly increases by an order of magnitude as the weight ratio of CoS_2 raises from 0 to 30%, demonstrating that CoS_2 –polysulfide interaction not only statically exists but also dynamically accelerates the electrochemical reactions of lithium polysulfides. In this case, CoS_2 particles that are attached to conductive graphene matrix provide access for electric charge to reach CoS_2 –polysulfide interface and to trigger polysulfide redox reactions. Such substantially facilitated charge transfer is adequately verified by electrochemical impedance spectra (EIS) of symmetrical cells (Figure 3b). The semicircle in the Nyquist plots, corresponding to the charge transfer resistance (R_{ct}) at electrode/polysulfide interfaces, remarkably shrank as CoS_2 incorporated. Detailed equivalent circuit and fitting results are listed in Figure S6 and Table S1. The R_{ct} is 1202 , 436 , and 116Ω for graphene, CoS_2 (15%) + G, and CoS_2 (30%) + G, respectively. Consequently, charge transfer at CoS_2 –polysulfide interface is much faster than at graphene–polysulfide interface, indicating considerable enhancement on redox kinetics of

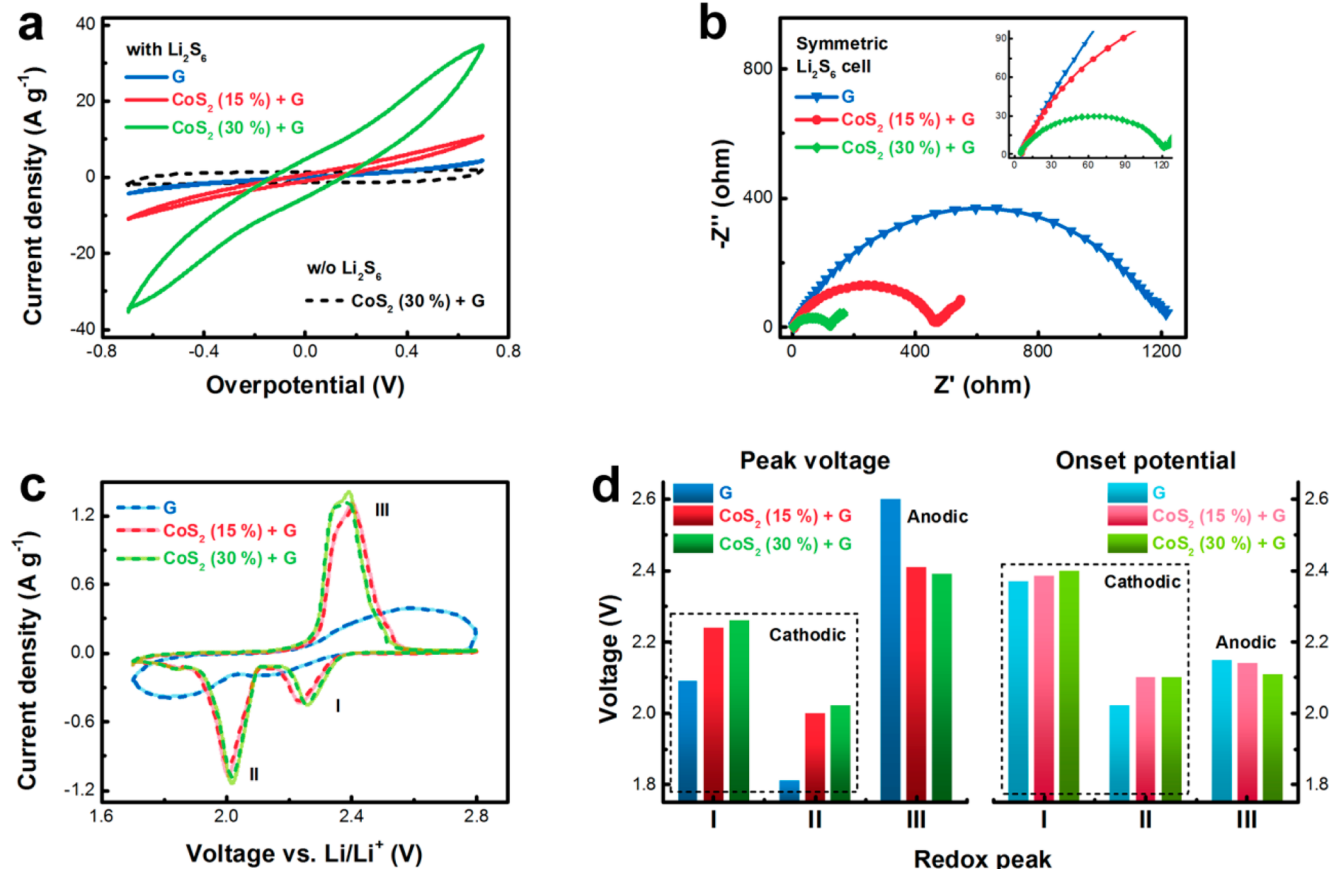


Figure 3. Dynamically enhanced polysulfide redox by CoS_2 . (a) Polarization curves and (b) EIS spectra of symmetrical Li_2S_6 – Li_2S_6 cells. (c) CV profiles, where the solid line refers to the first cycle and the dotted line refers to the second cycle, and (d) corresponding peak voltages and onset potentials of asymmetric Li–S cells. Different host materials of (1) G, (2) CoS_2 (15%) + G, and (3) CoS_2 (30%) + G are utilized.

polysulfides in liquid phase ($\text{Li}_2\text{S}_8 \leftrightarrow \text{Li}_2\text{S}_6 \leftrightarrow \text{Li}_2\text{S}_4$) by introducing highly sulfophilic CoS_2 hosts.

The accelerated polysulfide redox in aprotic electrolyte further affects the series of coupled liquid–solid conversion ($\text{S}_8 \leftrightarrow \text{Li}_2\text{S}_8$ and $\text{Li}_2\text{S}_4 \leftrightarrow \text{Li}_2\text{S}_2/\text{Li}_2\text{S}$), which is probed by CV profiles of Li–S batteries using different host materials (graphene, CoS_2 (15%) + G, and CoS_2 (30%) + G) (Figure 3c). 75 wt % sulfur was loaded on host materials via a typical melt-diffusion method (Figure S7). Consistent with aforementioned slow redox kinetics of polysulfides on graphene surface, pure graphene-based sulfur cathode exhibited broad cathodic and anodic peaks as well as severe polarization. Two cathodic peaks at 2.09 (I) and 1.81 (II) V and one anodic peak at 2.60 (III) V were observed for sulfur/graphene composite (S/G) cathode (Figure 3d). The incorporation of 15 wt % CoS_2 substantially mitigated polarization, raising cathodic peaks and reducing anodic peak by approximately 0.2 V. Two sharp cathodic peaks at ~2.25 and ~2.00 V can be noticed upon addition of CoS_2 , representing $\text{S}_8 \rightarrow \text{Li}_2\text{S}_4$ and $\text{Li}_2\text{S}_4 \rightarrow \text{Li}_2\text{S}_2/\text{Li}_2\text{S}$ reactions, respectively. On the anodic side, two corresponding peaks locating at 2.3–2.5 V overlaid with each other, accounting for the oxidation of Li_2S to polysulfides and sulfur. The second CV cycle also overlaps well with the first cycle, indicating a constant suppression on electrochemical polarization by incorporating sulfophilic CoS_2 hosts. Moreover, the electrocatalytic effect of CoS_2 is validated by the changes in onset potentials for all three redox peaks (Figure 3d and Table S2). The onset potential was taken at a current density of 10

$\mu\text{A cm}^{-2}$ beyond the baseline current, following a common definition employed in electrocatalysis. The detailed determination can be found in Figure S8. Generally, the incorporation of CoS_2 increases the onset potentials of cathodic peaks (I and II) while decreases that of the anodic peak with respect to the pure graphene electrode, verifying an accelerated kinetics over the CoS_2 electrocatalyst. Interestingly, note that there is remarkable decrease in polarization for liquid–solid conversion while it is polysulfide redox kinetics in liquid phase that is virtually enhanced upon the participation of CoS_2 , as demonstrated by results of symmetric cells. The reason why polarization diminishes for liquid–solid processes by accelerating liquid–liquid redox will be explained later.

As the result of the low annealing temperature (250 °C) for fabricating graphene, the control graphene sample has been proved to be functionalized with relatively richer oxygen groups than the sample prepared under higher annealing temperature (1000 °C), which is denoted as HT-G.⁴⁷ The surface functional groups are believed to enhance the dispersion of inorganic particles.⁴⁸ However, the incomplete removal of oxygen groups unambiguously results in more structural defects, which lowers the electrical conductivity and thereby could be one of the reasons why the polarization of S/G cathodes is severe. To validate the influence of oxygen functional groups, both CV test and corresponding calculation of onset potential were performed on HT-G/S cathode (Figure S9). Apparently, the polarization of HT-G sample is significantly reduced with respect to the G sample (Figure S9a). However, the onset

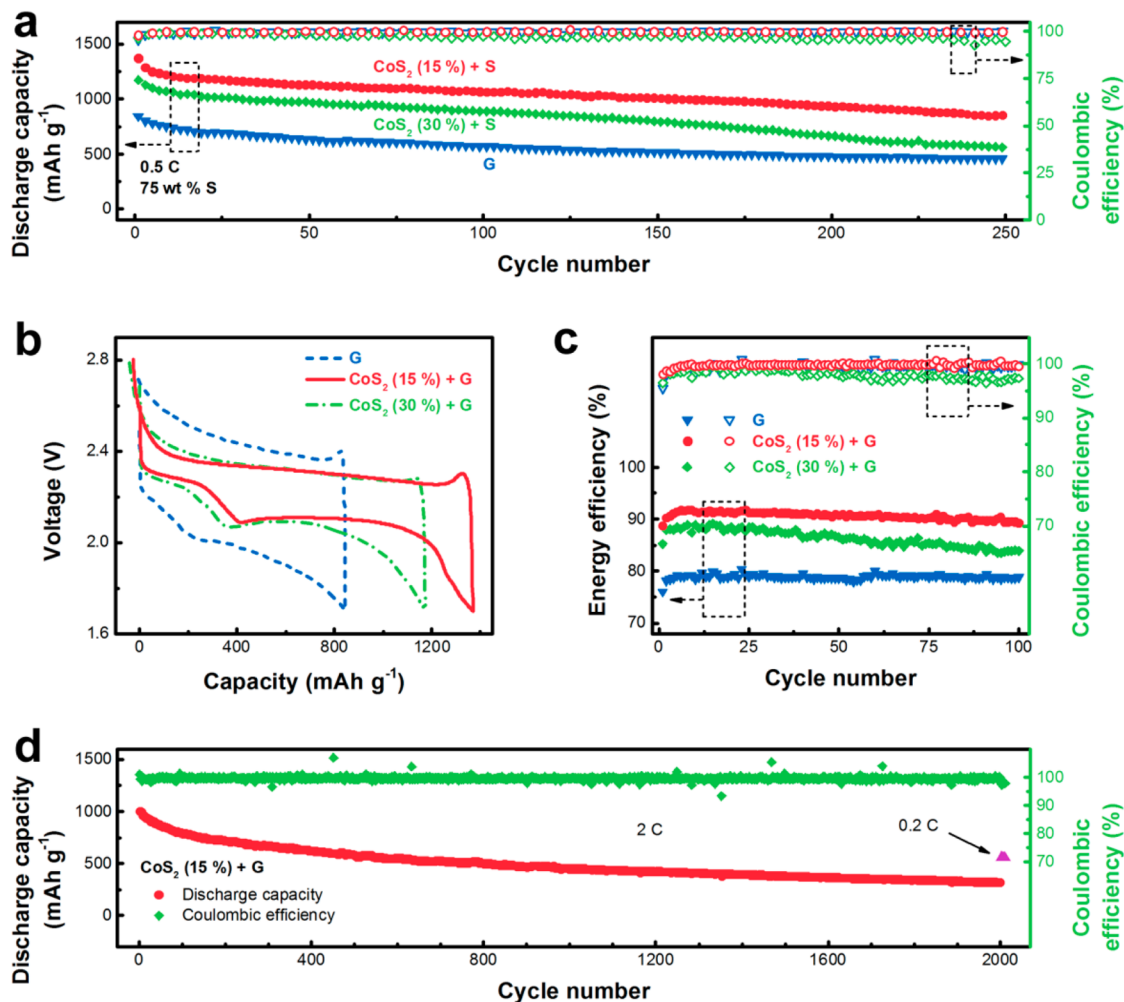


Figure 4. Electrochemical performance of S/G cathodes with or without CoS₂ addition. (a) Cycling performance, (b) galvanostatic charge–discharge profiles at 1st cycle, and (c) energy efficiency and Coulombic efficiency of graphene, CoS₂ (15%) + G, and CoS₂ (30%) + G-based sulfur cathode at current density of 0.5 C. (d) Cycling performance of CoS₂ (15%) + G-based sulfur cathode at a current density of 2.0 C for 2000 cycles, followed by 10 cycles at 0.2 C.

potentials of HT-G/S cathode are still worse than CoS₂-incorporated S/G cathodes for redox peak II and III (Figure S9b). The only exception is the redox peak I that is assigned to the conversion from solid sulfur to polysulfides. Furthermore, the onset potential of HT-G/S is even worse than the pristine G/S sample for charging the battery. All these results evidence that the charge and discharge may follow different reaction pathways and the surface polarity of the scaffolding materials leaves a more remarkable impact on the charging process. Future studies should be carried out to investigate such a different effect.

The electrochemical performance of CoS₂-incorporated S/G cathodes with enhanced polysulfide redox are probed as Figure 4. On account of the enhanced polysulfide redox kinetics by CoS₂, cyclic performances of composite cathodes are significantly improved. 75 wt % sulfur was incorporated as discussed above, with sulfur:graphene weight ratio of 4.3:1, 3.5:1, and 3:1 in S/CoS₂ (30%) + G, S/CoS₂ (15%) + G, and S/G cathodes, respectively. Significant promotion in discharge capacity can be achieved upon incorporation of CoS₂ at a current density of 0.5 C (1.0 C = 1672 mAh g⁻¹, based on the theoretical capacity of sulfur) (Figure 4a). Compared to the low discharge capacity of a pure S/G cathode (843 mAh g⁻¹ at first

cycle and 513 mAh g⁻¹ after 150 cycles), cathodes with CoS₂ exhibited much higher discharge capacity. An initial discharge capacity of 1174 mAh g⁻¹ was achieved using CoS₂ (30%) + G hosts, and an even higher 1368 mA h g⁻¹ for CoS₂ (15%) + G hosts, which was 62% higher than S/G cathode and accounted for 82% theoretical utilization of sulfur. A high capacity of 1005 mAh g⁻¹ was preserved after 150 cycles for CoS₂ (15%) + G hosts, almost twice as much as that of pure graphene counterpart. The corresponding capacity retention for S/CoS₂ (15%) + G and S/CoS₂ (30%) + G cathodes were also higher than the S/G cathode, indicating promoted cycling stability (Figure S10). Even HT-G with less defects and higher electrical conductivity than G is incomparable with CoS₂-based scaffolds, which is in good accordance with the analysis of onset potential (Figure S11). The abundant oxygen functional groups in G samples have been proved to be effective to suppress shuttle effect.⁴⁹ However, when a high sulfur content and a high current density are applied, the influence of electrical conductivity and electrochemical kinetics might be more significant than surface functionalities. The boost in discharge capacity can be attributed to enhanced polysulfide redox reactions that endow a high utilization of polysulfides as mobile redox materials.

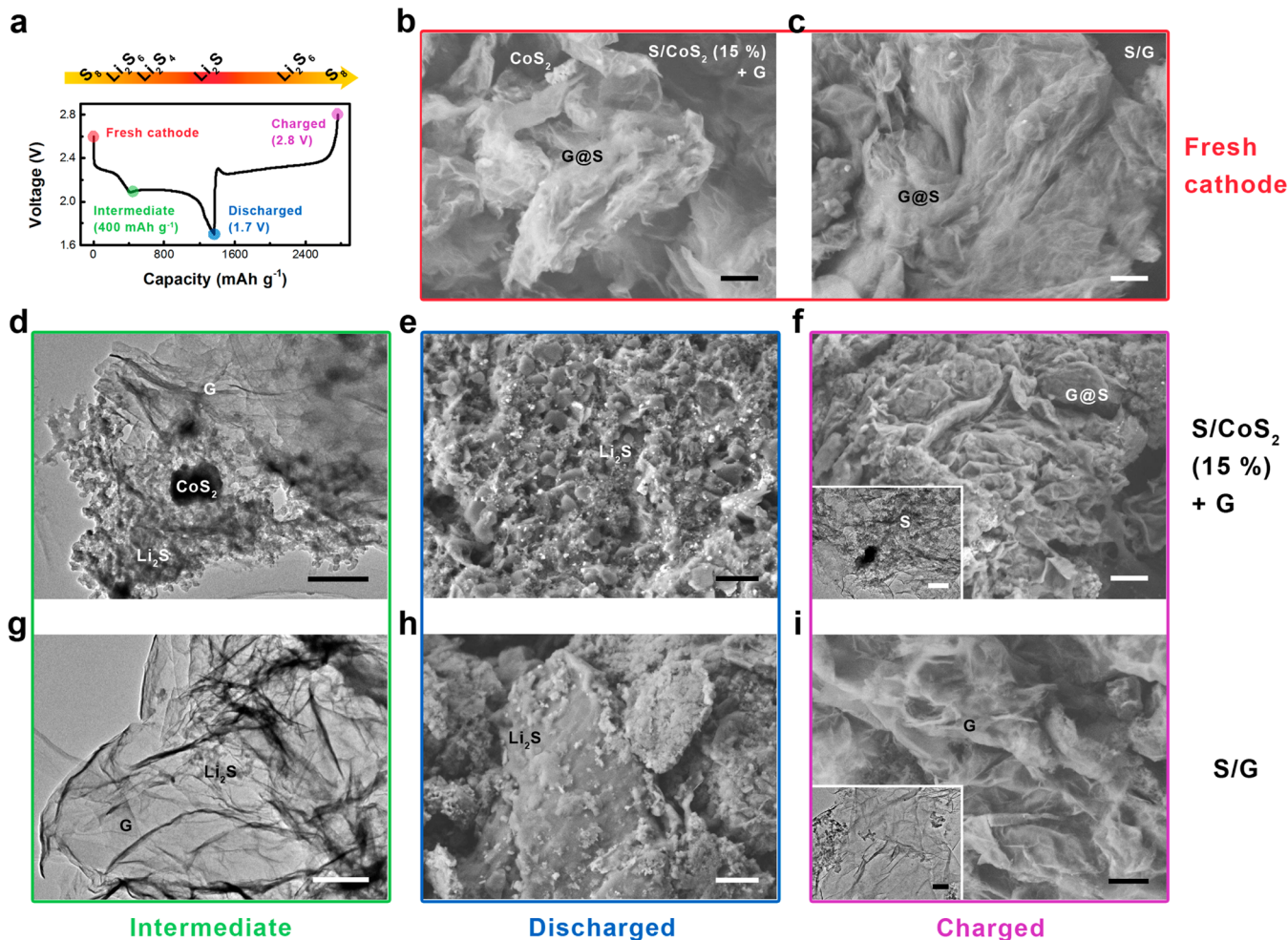


Figure 5. Morphological evolution of sulfur composite cathodes at different charge/discharge states. (a) The galvanostatic charge–discharge profile of the first cycle. As the colored dots indicated, fresh cathodes (red), cathodes at intermediate state (green, the beginning of the lower plateau where capacity reaches $\sim 400 \text{ mAh g}^{-1}$ for S/CoS_2 (15%) + G), cathodes at fully discharged state (blue, 1.7 V), and cathodes at fully charged states (purple, 2.8 V) are monitored by SEM. SEM images of fresh cathodes using (b) CoS_2 (15%) + G and (c) graphene as hosts. SEM images of S/CoS_2 (15%) + G at (d) intermediate, (e) discharged, and (f) charged states., and SEM images of S/G at (g) intermediate, (h) discharged, and (i) charged states. Scale bars, (b, c, e, h) 1 μm ; (d, g) 500 nm; (f, i) 1 μm and 200 nm (inset).

Consistent with the CV profiles, CoS_2 induced smaller polarizations at all charge or discharge plateaus, indicating a much promoted redox kinetics (Figure 4b). The alleviated voltage hysteresis led to improved energy efficiency. Rather than Coulombic efficiency which only represents the ratio of charge output/input ($Q = \int U I \, dt$), energy efficiency, taking account of voltage polarization ($E = \int U I \, dt$), is a more crucial indicator for sustainable large-scale energy storage systems. The small gap between charge and discharge voltages was realized by the addition of CoS_2 , resulting in promoted energy efficiency, from 80% up to nearly 90% (Figure 4c). The significant improvement in energy efficiency is crucial for integrating Li–S batteries in high-efficiency grid applications. Reduced voltage hysteresis and enhanced specific capacity were achieved using CoS_2 (15%) + G hosts at various rates of 0.2, 0.5, 1.0, and 2.0 C as well, indicating significantly enhanced polysulfide electrochemical reactions (Figure S12).

A discharge capacity of 1003 mA h g^{-1} was delivered for the S/CoS_2 (15%) + G cathode at 2.0 C in the first cycle, and 32% was maintained after 2000 cycles, providing a low capacity decay rate of 0.034%/cycle (Figure 4d). After prolonged 2000 cycles at 2.0 C, a stable capacity at 554 mA h g^{-1} were achieved

at a low current density of 0.2 C, demonstrating the robust nature of S/CoS_2 + G cathodes. High energy densities of 1425 and 1071 W h kg^{-1} were available at power densities of 0.88 and 3.5 kW kg^{-1} for $\text{Li}||\text{S}/\text{CoS}_2$ (15%) + G batteries based on the weight of lithium, sulfur, carbon, CoS_2 , and binder. As the result of the relatively low sulfur loading (0.4 mg cm^{-2}), the practical energy density is undesirable (129 W h kg^{-1}) if the weight of aluminum current collector ($\sim 4 \text{ mg cm}^{-2}$) is considered. However, such a defect can be offset by employing a lighter current collector without the assist of carbon blacks and binders (carbon nanotube paper, $\sim 1 \text{ mg cm}^{-2}$)¹⁸ and increasing the areal sulfur loading amount to 2.9 mg cm^{-2} . The high-sulfur-loading electrode exhibited a high capacity of 1131 mAh g^{-1} at 0.1 C, which corresponds to an energy density of 1098 Wh kg^{-1} based on all the components except for the separator and electrolyte (Figure S13). We believe that more superior energy density for the whole device can be promised by other advanced flexible current collectors such as graphene films or three-dimensional graphene foam that are light and conductive.^{15,16,50}

Note that CoS_2 was available for lithium storage.⁵¹ However, CoS_2 herein possessed a reversible capacity of 120 mA h g^{-1}

(based on CoS_2 weight) with the same working condition in ether-based electrolytes, which only contributed less than 3% of overall capacity (**Figure S14**). In summary, the CoS_2 virtually benefits the overall energy density, power density, and cyclic stability of a Li–S battery.

For tackling the issue of polysulfide flooding, encapsulation or adsorption strategies were widely accepted to minimize the dissolution of polysulfides through either physical confinement provided by nanostructured materials^{14,39,52} or chemical immobilization afforded by functionalization or heteroatom doping.^{19,46,53,54} However, in principle, when a polysulfide molecule is generated on the electrode, there are two endings: one is its detachment from the electrode, resulting in electrical insulation; the other is its conversion to a lower-order polysulfide molecule and subsequent formation of solid deposits. Compared to tuning the dissolvability and transport behavior of polysulfides in aprotic electrolytes, manipulating the redox reactivity of polysulfides upon conducting surface has been rarely concerned. Actually, the liquid transformation of high-polar polysulfides and corresponding charge transfer is kinetically sluggish due to the poor affinity of polysulfides to nonpolar carbon electrode materials that is conventionally employed. When graphene was used as host materials, the R_{ct} of a symmetric Li_2S_6 – Li_2S_6 cell (1202Ω) was much larger than symmetric cells of S–S pair (580Ω) and Li_2S – Li_2S pair (365Ω), indicating the rate-controlled step of liquid–liquid conversion ($\text{Li}_2\text{S}_8 \leftrightarrow \text{Li}_2\text{S}_6 \leftrightarrow \text{Li}_2\text{S}_4$) in the whole redox (**Figure S15**). The differences in the diffusion process could be depicted by Warburg impedance:⁵⁵

$$Z_w = \sigma/\omega^{1/2} - j\sigma/\omega^{1/2} \quad (\text{Warburg impedance } Z_w)$$

$$\sigma = \frac{RT}{n^2 F^2 A \sqrt{2}} \left(\frac{1}{C_{\text{ox}}^{\text{b}} \sqrt{D_{\text{ox}}}} + \frac{1}{C_{\text{re}}^{\text{b}} \sqrt{D_{\text{re}}}} \right)$$

(Warburg coefficient σ)

where the Warburg coefficient is affected by number of electron transfer (n), surface area of reaction (A), bulk concentrations of the oxidant and reductant ($C_{\text{ox/re}}$), and their diffusivities ($D_{\text{ox/re}}$). It is difficult to precisely probe the exact diffusion behaviors. However, by fitting the data using equivalent circuit shown in **Figure S6**, it can be derived that Warburg coefficient σ for S–S, Li_2S_6 – Li_2S_6 , and Li_2S – Li_2S symmetrical cells are 358.5, 24.7, and $243.2 \Omega \text{ s}^{-1/2}$, respectively. The relatively lower σ for the Li_2S_6 – Li_2S_6 symmetrical cell can be qualitatively explained by higher concentration of soluble reactants in the liquid phase, namely, higher C_{ox}^{b} and C_{re}^{b} . It can be deduced that, even though the concentration of reactants is higher in the Li_2S_6 – Li_2S_6 symmetrical cell, there is more considerable impedance for the liquid–liquid reaction as indicated by the larger R_{ct} . Therefore, the liquid–liquid process of sulfur species is the kernel of sulfur redox chemistry (**Figure 1a**).

In a typical discharge–charge cycle, the transition of polysulfide redox in aprotic electrolytes connects the two solid phases: sulfur and Li_2S (**Figure 5a**). In this contribution, CoS_2 was engineered to provide strong CoS_2 –polysulfide interaction and to facilitate the liquid–liquid redox, further affecting the correlated liquid–solid transformation. Due to the extremely low specific surface area of CoS_2 , it is unavailable for solid sulfur species (S_8 , Li_2S_2 / Li_2S) to deposit on the surface of CoS_2 . However, the solid–liquid transformation can be accelerated by speeding up reactions of liquid intermediates.

For instance, Li_2S_4 is easily oxidized to Li_2S_6 under the assistance of heteropolar CoS_2 , inducing higher molar ratio of Li_2S_6 / Li_2S_4 . On the one hand, the decreased Li_2S_4 concentration favors Li_2S oxidation reaction thermodynamically. On the other hand, adequate Li_2S_6 comproportionates with Li_2S into Li_2S_4 via a nonelectrochemical process. Hence, the solid–liquid transformation from Li_2S to Li_2S_4 is indirectly accelerated by CoS_2 . For its reverse process, the formation of Li_2S from polysulfides is also promoted. It is previously confirmed by operando X-ray absorption spectroscopy that Li_2S_6 , Li_2S_4 , and Li_2S coexist at lower discharge plateau.⁵⁶ Li_2S_4 concentration remains relatively stable to keep constant voltage, while Li_2S_6 could be regarded as “ Li_2S_4 reserve”. CoS_2 relieves the kinetic barrier from Li_2S_6 to Li_2S_4 , promises smooth polysulfide redox transformation, and thus allows polysulfides to reach dynamic equilibrium and to form Li_2S_4 -enriched area around CoS_2 , which is beneficial for Li_2S nucleation and growth. Similarly, $\text{S}_8 \rightarrow \text{Li}_2\text{S}_8$ reduction could be expedited by catalyzing the conversion from Li_2S_8 to short chain polysulfides (Li_2S_6 and Li_2S_4). In reverse, while Li_2S_8 has been reported to be thermodynamically unstable and kinetically inaccessible in ether-based electrolyte, which inhibits the full conversion from lithium polysulfides to elemental sulfur,⁵⁷ CoS_2 can enrich the metastable Li_2S_8 on the electrode surface by catalyzing liquid process of $\text{Li}_2\text{S}_6 \rightarrow \text{Li}_2\text{S}_8$ and stabilize the surface reaction for full conversion to sulfur. Overall speaking, the acceleration of the core step, namely liquid–liquid redox of polysulfides, by introducing sulfophilic CoS_2 to form high-efficient charge-transfer junction ignites the whole solid–liquid–solid electrochemistry of sulfur in an aprotic electrolyte.

The morphologies of cycled cathodes at different states were monitored to well validate the above-discussed electrochemical mechanisms. Accordingly, we endow CoS_2 several attributes for tuning the sulfur electrochemistry: (1) CoS_2 does not hinder the intimate contact between sulfur and graphene substrates since CoS_2 only contribute tiny conductive surface (**Figure 5b,c**). (2) The sequence of Li_2S formation is accelerated by CoS_2 . At the beginning of the lower plateau, substantial Li_2S particles deposits on the graphene substrate surrounding the CoS_2 (**Figure 5d**). Once Li_2S nucleates upon graphene, its polar surface can adsorb polysulfides, expedites electrodeposition of Li_2S_4 , and enables subsequent growth of Li_2S as HR-TEM images indicated (**Figure S16**). On the contrary, only negligible small clusters of Li_2S is formed on bare graphene supports (**Figure 5g**). (3) Incorporating CoS_2 enriches the surface concentration of Li_2S_4 and elevates the density of Li_2S nuclei, which favors the controllable growth of Li_2S . At fully discharged state, the graphene flake is carpeted with fish-scale-like CoS_2 nanoparticles with size no larger than $1 \mu\text{m}$ (**Figure 5e**). However, in S/G cathode, Li_2S is deposited consecutively into bulk particles, which can be attributed to the low and declining surface concentration of Li_2S_4 without the assistance of CoS_2 (**Figure 5h**). The morphological difference is in good accordance with limited capacity and downward sloping lower discharging voltage of S/G cathodes (**Figure 4b**). (4) CoS_2 favors the full conversion to elemental sulfur during charging via propelled adsorbate–adsorbate conversion from Li_2S_6 into metastable Li_2S_8 and surface stabilization. In the charged S/ CoS_2 (15%) + G cathode, graphene is conformally coated by sulfur and exhibits thick flakes and rough surface (**Figure 5f**). While in charged S/G cathode, the graphene flake is thin and clean, indicating a restrained charging process (**Figure 5i**). These merits of CoS_2 for sulfur electrochemistry reflected on

not only promoted capacity and reduced polarization of Li–S batteries at high current density, but also the cyclic stability at low current density. Though initial capacities are similar for S/G and S/CoS₂ (30%) + G cathodes at 0.2 C, the stability of CoS₂-incorporated materials is much better (Figure S17). Considering the fact that CoS₂ herein employed is in the bulk form, we thought that there should be many efforts to optimize the structure and properties of CoS₂ for further enhancement, including crystalline form, exposed facets, heteroatom doping, support interaction, and percentage in the hybrids.

Recently, inorganic host materials are gaining increasing attention as the insights into sulfur redox chemistry is developed. Inorganic materials such as SiO₂,⁴⁵ TiO₂,^{58,59} Ti₄O₇,^{35,60} MnO₂,³⁶ Co₉S₈,⁴¹ Al₂O₃,⁶¹ MXene,⁶² and Mg_{0.6}Ni_{0.4}O,⁶³ as well as metal–organic frameworks⁶⁴ were used as either porous reservoirs for polysulfides or encapsulation shells, which thereafter scaled to conducting yet inorganic materials including 2D layered carbides or sulfides for further enhancing the battery performance. However, these advancements still focused on strengthening the adsorption by strong chemical interaction and rarely demonstrated electrocatalytic effects for enhancing polysulfide redox. Only few examples such as Magnéli-phase Ti₄O₇^{35,60} and birnessite MnO₂ nanosheets³⁶ elaborated a tailored sulfur electrochemistry toward upgraded activity of polar sulfur species. The use of synergistic dual-interaction based on S_n²⁻ → Co^{δ+} and Li⁺ → S^{δ-} is very effective to build superior LiPS adsorptivity of Co₉S₈ and render the high sulfur loading electrodes (up to 4.5 mg cm⁻² loading) with stable cycling over 150 cycles in a Li–S cell.⁴¹ However, their performance depended on not only their high-polar nature but also high surface area (>200 m² g⁻¹) since no carbon support was integrated. Synthesizing inorganic crystals with high surface area and conductivity is virtually challenging, and the high-rate capability is thereby retarded. Hybridization of inorganic materials such as ITO with carbon nanomaterials is a compromising but effective approach.³⁷ But the high cost of ITO hinders its bulk applications. Therefore, a cost-effective, nonporous mineral of CoS₂ without sophisticated synthetic route and in its bulk form was herein selected as electrocatalysts for polysulfide redox in the aprotic electrolyte. The positive impact of graphene is also notable. As CoS₂ weight ratio increases from 15 to 30%, the redox activity of polysulfides increases likewise (Figure 3a), but the capacity, energy efficiency, and cyclic stability are curtailed (Figure 4a,b), demonstrating the non-negligible role of graphene for supporting solid sulfur species. Carbon nanomaterials should still exert their virtue of lightweight, high surface area, and large pore volume for accommodating solid deposits of sulfur/Li₂S though they are unfavorable for polysulfide redox. Nevertheless, the correlation shown in Figure S18 indicates that the CoS₂/graphene hybrid system has a higher specific capacity per unit surface area than pure graphene, demonstrating a higher electrochemical activity of Li–S redox that is supposed to be propelled by the electrocatalytic effect of sulfophilic hosts. Thus, hybrid materials of carbon and earth-abundant electrocatalysts such as CoS₂ might be superb for the full solid–liquid–solid sulfur redox. Yet the structure and chemistry of as-synthesized CoS₂ has not been elaborately mediated; further enhancement should be on the way: (1) understanding the impact of electronic structure on polysulfide redox; (2) reducing the dimension of electrocatalysts to maximize exposed polar surface; (3) engineering the crystal facets of inorganic

compounds to mediate the adsorbate–adsorbent interaction; (4) exploring stronger ionic crystals; and (5) introducing strong-coupled effect between substrates and supported inorganic materials for intriguing modulation of material properties.

In conclusion, CoS₂ was proved to be an efficient additive into carbon/sulfur composite cathodes, managing to achieve higher discharge capacity at high rates, to improve energy efficiency, and to enhance cycling stability. There were not only strongly coupled CoS₂–polysulfide interaction, but also dynamically enhanced polysulfide redox reactions, confirmed by both theoretical and experimental results. The significantly enhanced polysulfide redox validly facilitated preceding solid–liquid and consequent liquid–solid processes, mitigating polarization among the whole sulfur redox chemistry. Though composited within cathode material in a simple, mechanical way and endowed with rather low specific surface area, CoS₂ particles generated magical effect on routine sulfur/graphene cathodes, raising discharge capacity by 60% and energy efficiency by 10% while realizing a slow capacity decay rate of 0.034%/cycle at 2.0 C. The concise yet effective modification of sulfur cathodes sheds light on the redox chemistry of sulfur species and realizes an accessible but efficient approach to improve the overall performance of Li–S batteries. Since the propelling redox reaction is not limited to Li–S system, we foresee a new branch of chemistry evolving in the area of high-power devices through the systems with controllable redox reactions. Further improvement could be anticipated by engineering inorganics in the view of modulating the strength and dynamic properties of inorganic host/polysulfide electrolyte redox couples for advanced energy storage.

■ ASSOCIATED CONTENT

§ Supporting Information

The Supporting Information is available free of charge on the ACS Publications website at DOI: [10.1021/acs.nanolett.5b04166](https://doi.org/10.1021/acs.nanolett.5b04166).

Experimental details, structure characterization, and electrochemical properties of CoS₂ + based electrode, along with additional supporting data ([PDF](#))

■ AUTHOR INFORMATION

Corresponding Author

*E-mail: zhang-qiang@mails.tsinghua.edu.cn (Q. Zhang).

Author Contributions

Z.Y., H.-J.P., and T.-Z.H. contributed equally to the work.

Notes

The authors declare no competing financial interest.

■ ACKNOWLEDGMENTS

This work was supported by funding from the Natural Scientific Foundation of China (No. 21306103, 21422604, and 21561130151), the National Basic Research Program of China (2015CB932500), Tsinghua University Initiative Scientific Research Program (2014z22076), and Tsinghua National Laboratory for Information Science and Technology. We thank the CV test of graphene sample by Wen-Tao Xu and helpful discussion from Lin Zhu, Rui Zhang, and Chen-Zi Zhao.

■ REFERENCES

- Bruce, P. G.; Freunberger, S. A.; Hardwick, L. J.; Tarascon, J.-M. *Nat. Mater.* **2011**, *11*, 19–29.

- (2) Manthiram, A.; Chung, S.-H.; Zu, C. *Adv. Mater.* **2015**, *27*, 1980–2006.
- (3) Yin, Y.-X.; Xin, S.; Guo, Y.-G.; Wan, L.-J. *Angew. Chem., Int. Ed.* **2013**, *52*, 13186–13200.
- (4) Zhang, S. *S. J. Power Sources* **2013**, *231*, 153–162.
- (5) Song, M.-K.; Cairns, E. J.; Zhang, Y. *Nanoscale* **2013**, *5*, 2186–2204.
- (6) Pope, M. A.; Aksay, I. A. *Adv. Energy Mater.* **2015**, *5*, 1500124.
- (7) Wang, D.-W.; Zeng, Q.; Zhou, G.; Yin, L.; Li, F.; Cheng, H.-M.; Gentle, I. R.; Lu, G. Q. *M. J. Mater. Chem. A* **2013**, *1*, 9382–9394.
- (8) Li, Z.; Huang, Y. M.; Yuan, L. X.; Hao, Z. X.; Huang, Y. H. *Carbon* **2015**, *92*, 41–63.
- (9) Ji, X.; Lee, K. T.; Nazar, L. F. *Nat. Mater.* **2009**, *8*, 500–506.
- (10) Lee, J. T.; Zhao, Y.; Thieme, S.; Kim, H.; Oschatz, M.; Borchardt, L.; Magasinski, A.; Cho, W.-I.; Kaskel, S.; Yushin, G. *Adv. Mater.* **2013**, *25*, 4573–4579.
- (11) Miao, L.-X.; Wang, W.-K.; Wang, A.-B.; Yuan, K.-G.; Yang, Y.-S. *J. Mater. Chem. A* **2013**, *1*, 11659–11664.
- (12) Zhao, M.-Q.; Sedran, M.; Ling, Z.; Lukatskaya, M. R.; Mashtalir, O.; Ghidiu, M.; Dyatkin, B.; Tallman, D. J.; Djenizian, T.; Barsoum, M. W.; Gogotsi, Y. *Angew. Chem., Int. Ed.* **2015**, *54*, 4810–4814.
- (13) Wang, H.; Yang, Y.; Liang, Y.; Robinson, J. T.; Li, Y.; Jackson, A.; Cui, Y.; Dai, H. *Nano Lett.* **2011**, *11*, 2644–2647.
- (14) Zhao, M.-Q.; Zhang, Q.; Huang, J.-Q.; Tian, G.-L.; Nie, J.-Q.; Peng, H.-J.; Wei, F. *Nat. Commun.* **2014**, *5*, 3410.
- (15) Zhou, G. M.; Pei, S.; Li, L.; Wang, D.-W.; Wang, S.; Huang, K.; Yin, L.-C.; Li, F.; Cheng, H.-M. *Adv. Mater.* **2014**, *26*, 625–631.
- (16) Zhou, G. M.; Paek, E.; Hwang, G. S.; Manthiram, A. *Nat. Commun.* **2015**, *6*, 7760.
- (17) Cheng, X.-B.; Huang, J.-Q.; Zhang, Q.; Peng, H.-J.; Zhao, M.-Q.; Wei, F. *Nano Energy* **2014**, *4*, 65–72.
- (18) Yuan, Z.; Peng, H.-J.; Huang, J.-Q.; Liu, X.-Y.; Wang, D.-W.; Cheng, X.-B.; Zhang, Q. *Adv. Funct. Mater.* **2014**, *24*, 6105–6112.
- (19) Peng, H.-J.; Hou, T.-Z.; Zhang, Q.; Huang, J.-Q.; Cheng, X.-B.; Guo, M.-Q.; Yuan, Z.; He, L.-Y.; Wei, F. *Adv. Mater. Interfaces* **2014**, *1*, 1400227.
- (20) Yang, Y.; Yu, G.; Cha, J. J.; Wu, H.; Vosgueritchian, M.; Yao, Y.; Bao, Z.; Cui, Y. *ACS Nano* **2011**, *5*, 9187–9193.
- (21) Zhou, W.; Yu, Y.; Chen, H.; DiSalvo, F. J.; Abruna, H. D. *J. Am. Chem. Soc.* **2013**, *135*, 16736–16743.
- (22) Wang, J.; He, Y.-S.; Yang, J. *Adv. Mater.* **2015**, *27*, 569–575.
- (23) Zhao, M.-Q.; Liu, X.-F.; Zhang, Q.; Tian, G.-L.; Huang, J.-Q.; Zhu, W.; Wei, F. *ACS Nano* **2012**, *6*, 10759–10769.
- (24) Yang, X.; Zhang, L.; Zhang, F.; Huang, Y.; Chen, Y. *ACS Nano* **2014**, *8*, 5208–5215.
- (25) Deng, Z.; Zhang, Z.; Lai, Y.; Liu, J.; Li, J.; Liu, Y. *J. Electrochem. Soc.* **2013**, *160*, A553–A558.
- (26) Mikhaylik, Y. V.; Akridge, J. R. *J. Electrochem. Soc.* **2004**, *151*, A1969–A1976.
- (27) Yao, H.; Yan, K.; Li, W.; Zheng, G.; Kong, D.; Seh, Z. W.; Narasimhan, V. K.; Liang, Z.; Cui, Y. *Energy Environ. Sci.* **2014**, *7*, 3381–3390.
- (28) Huang, J.-Q.; Zhuang, T.-Z.; Zhang, Q.; Peng, H.-J.; Chen, C.-M.; Wei, F. *ACS Nano* **2015**, *9*, 3002–3011.
- (29) Peng, H.-J.; Wang, D.-W.; Huang, J.-Q.; Cheng, X.-B.; Yuan, Z.; Wei, F.; Zhang, Q. *Adv. Sci.* **2016**, *3*, 1500268.
- (30) Huang, J.-Q.; Zhang, Q.; Peng, H.-J.; Liu, X.-Y.; Qian, W.-Z.; Wei, F. *Energy Environ. Sci.* **2014**, *7*, 347–353.
- (31) Aurbach, D.; Pollak, E.; Elazari, R.; Salitra, G.; Kelley, C. S.; Affinito, J. *J. Electrochem. Soc.* **2009**, *156*, A694–A702.
- (32) Wu, F.; Qian, J.; Chen, R.; Lu, J.; Li, L.; Wu, H.; Chen, J.; Zhao, T.; Ye, Y.; Amine, K. *ACS Appl. Mater. Interfaces* **2014**, *6*, 15542–15549.
- (33) Suo, L.; Hu, Y.-S.; Li, H.; Armand, M.; Chen, L. *Nat. Commun.* **2013**, *4*, 1481.
- (34) Lin, Z.; Liu, Z.; Dudney, N. J.; Liang, C. *ACS Nano* **2013**, *7*, 2829–2833.
- (35) Pang, Q.; Kundu, D.; Cuisinier, M.; Nazar, L. F. *Nat. Commun.* **2014**, *5*, 4759.
- (36) Liang, X.; Hart, C.; Pang, Q.; Garsuch, A.; Weiss, T.; Nazar, L. F. *Nat. Commun.* **2015**, *6*, 5682.
- (37) Yao, H.; Zheng, G.; Hsu, P.-C.; Kong, D.; Cha, J. J.; Li, W.; Seh, Z. W.; McDowell, M. T.; Yan, K.; Liang, Z.; Narasimhan, V. K.; Cui, Y. *Nat. Commun.* **2014**, *5*, 3943.
- (38) Wang, H.; Zhang, Q.; Yao, H.; Liang, Z.; Lee, H.-W.; Hsu, P.-C.; Zheng, G.; Cui, Y. *Nano Lett.* **2014**, *14*, 7138–7144.
- (39) Seh, Z. W.; Yu, J. H.; Li, W.; Hsu, P.-C.; Wang, H.; Sun, Y.; Yao, H.; Zhang, Q.; Cui, Y. *Nat. Commun.* **2014**, *5*, 5017.
- (40) Fan, F. Y.; Carter, W. C.; Chiang, Y.-M. *Adv. Mater.* **2015**, *27*, 5203–5209.
- (41) Pang, Q.; Kundu, D.; Nazar, L. F. *Mater. Horiz.* **2016**, DOI: 10.1039/C5MH00246J.
- (42) Ogawa, S.; Teranishi, T. *Phys. Lett. A* **1972**, *42*, 147–148.
- (43) Faber, M. S.; Park, K.; Cabán-Acevedo, M.; Santra, P. K.; Jin, S. *J. Phys. Chem. Lett.* **2013**, *4*, 1843–1849.
- (44) Faber, M. S.; Dziedzic, R.; Lukowski, M. A.; Kaiser, N. S.; Ding, Q.; Jin, S. *J. Am. Chem. Soc.* **2014**, *136*, 10053–10061.
- (45) Ji, X.; Evers, S.; Black, R.; Nazar, L. F. *Nat. Commun.* **2011**, *2*, 325.
- (46) Song, J.; Gordin, M. L.; Xu, T.; Chen, S.; Yu, Z.; Sohn, H.; Lu, J.; Ren, Y.; Duan, Y.; Wang, D. *Angew. Chem., Int. Ed.* **2015**, *54*, 4325–4329.
- (47) Chen, C.-M.; Zhang, Q.; Yang, M.-G.; Huang, C.-H.; Yang, Y.-G.; Wang, M.-Z. *Carbon* **2012**, *50*, 3572–3584.
- (48) Liu, J.; Yang, T. Y.; Wang, D. W.; Lu, G. Q. M.; Zhao, D. Y.; Qiao, S. Z. *Nat. Commun.* **2013**, *4*, 2798.
- (49) Ji, L.; Rao, M.; Zheng, H.; Zhang, L.; Li, Y.; Duan, W.; Guo, J.; Cairns, E. J.; Zhang, Y. *J. Am. Chem. Soc.* **2011**, *133*, 18522–18525.
- (50) Zhou, G.; Li, L.; Ma, C.; Wang, S.; Shi, Y.; Koratkar, N.; Ren, W.; Li, F.; Cheng, H.-M. *Nano Energy* **2015**, *11*, 356–365.
- (51) Xie, J.; Liu, S.; Cao, G.; Zhu, T.; Zhao, X. *Nano Energy* **2013**, *2*, 49–56.
- (52) Li, L.; Ruan, G.; Peng, Z.; Yang, Y.; Fei, H.; Raji, A. R.; Samuel, E. L.; Tour, J. M. *ACS Appl. Mater. Interfaces* **2014**, *6*, 15033–15039.
- (53) Song, J.; Xu, T.; Gordin, M. L.; Zhu, P.; Lv, D.; Jiang, Y.-B.; Chen, Y.; Duan, Y.; Wang, D. *Adv. Funct. Mater.* **2014**, *24*, 1243–1250.
- (54) Zhou, G. M.; Zhao, Y.; Manthiram, A. *Adv. Energy Mater.* **2015**, *5*, 1402263.
- (55) Levi, M. D.; Salitra, G.; Markovsky, B.; Teller, H.; Aurbach, D.; Heider, U.; Heider, L. *J. Electrochem. Soc.* **1999**, *146*, 1279–1289.
- (56) Cuisinier, M.; Cabelguen, P.-E.; Evers, S.; He, G.; Kolbeck, M.; Garsuch, A.; Bolin, T.; Balasubramanian, M.; Nazar, L. F. *J. Phys. Chem. Lett.* **2013**, *4*, 3227–3232.
- (57) Chen, J.-J.; Yuan, R.-M.; Feng, J.-M.; Zhang, Q.; Huang, J.-X.; Fu, G.; Zheng, M.-S.; Ren, B.; Dong, Q.-F. *Chem. Mater.* **2015**, *27*, 2048–2055.
- (58) Seh, Z. W.; Li, W.; Cha, J. J.; Zheng, G.; Yang, Y.; McDowell, M. T.; Hsu, P.-C.; Cui, Y. *Nat. Commun.* **2013**, *4*, 1331.
- (59) Xiao, Z.; Yang, Z.; Wang, L.; Nie, H.; Zhong, M. E.; Lai, Q.; Xu, X.; Zhang, L.; Huang, S. *Adv. Mater.* **2015**, *27*, 2891–2898.
- (60) Tao, X.; Wang, J.; Ying, Z.; Cai, Q.; Zheng, G.; Gan, Y.; Huang, H.; Xia, Y.; Liang, C.; Zhang, W.; Cui, Y. *Nano Lett.* **2014**, *14*, 5288–5294.
- (61) Han, X.; Xu, Y.; Chen, X.; Chen, Y.-C.; Weadock, N.; Wan, J.; Zhu, H.; Liu, Y.; Li, H.; Rubloff, G.; Wang, C.; Hu, L. *Nano Energy* **2013**, *2*, 1197–1206.
- (62) Liang, X.; Garsuch, A.; Nazar, L. F. *Angew. Chem., Int. Ed.* **2015**, *54*, 3907–3911.
- (63) Zhang, Y.; Zhao, Y.; Yermukhametova, A.; Bakenov, Z.; Chen, P. *J. Mater. Chem. A* **2013**, *1*, 295–301.
- (64) Zheng, J.; Tian, J.; Wu, D.; Gu, M.; Xu, W.; Wang, C.; Gao, F.; Engelhard, M. H.; Zhang, J.-G.; Liu, J.; Xiao, J. *Nano Lett.* **2014**, *14*, 2345–2352.